NANO LETTERS

2007
Vol. 7, No. 10
3157−3164

On the Quenching of Semiconductor Quantum Dot Photoluminescence by Proximal Gold Nanoparticles

Thomas Pons,[†,‡,§] Igor L. Medintz,*[,†,||] Kim E. Sapsford,[||,⊥] Seiichiro Higashiya,[#] Amy F. Grimes,[+] Doug S. English,[+] and Hedi Mattoussi*[,§]

U.S. Naval Research Laboratory, Division of Optical Sciences, Washington, D.C. 20375, U.S. Naval Research Laboratory, Center for Bio/Molecular Science and Engineering, Washington, D.C. 20375, George Mason University, Manassas, Virginia 21220, Department of Chemistry, University of Albany, State University of New York, Albany, New York 12222, and Department of Chemistry and Biochemistry, University of Maryland, College Park, Maryland 20742

Received July 17, 2007; Revised Manuscript Received August 20, 2007

ABSTRACT

Luminescent quantum dots (QDs) were proven to be very effective fluorescence resonance energy transfer donors with an array of organic dye acceptors, and several fluorescence resonance energy transfer based biosensing assemblies utilizing QDs have been demonstrated in the past few years. Conversely, gold nanoparticles (Au-NPs) are known for their capacity to induce strong fluorescence quenching of conventional dye donors. Using a rigid variable-length polypeptide as a bifunctional biological linker, we monitor the photoluminescence quenching of CdSe–ZnS QDs by Au-NP acceptors arrayed around the QD surface, where the center-to-center separation distance was varied over a broad range of values (∼50–200 Å). We measure the Au-NP-induced quenching rates for such QD conjugates using steady-state and time-resolved fluorescence measurements and examine the results within the context of theoretical treatments based on the Förster dipole–dipole resonance energy transfer, dipole–metal particle energy transfer, and nanosurface energy transfer. Our results indicate that nonradiative quenching of the QD emission by proximal Au-NPs is due to long-distance dipole–metal interactions that extend significantly beyond the classical Förster range, in agreement with previous studies using organic dye–Au-NP donor–acceptor pairs.

Introduction and Background. Due to their unique optical and spectroscopic properties, luminescent semiconductor quantum dots (QDs) have proven to be very effective donor fluorophores in an array of processes and bioassays based on fluorescence resonance energy transfer (FRET).[1−4] In particular, the combination of broad absorption coupled with size-tunable photoluminescence (PL) and larger physical size (compared to conventional dyes) allows: (1) optimization of the spectral overlap with any potential FRET acceptor; (2) excitation at a wavelength far removed from the acceptor absorption peak, minimizing acceptor direct excitation; and (3) the ability to array multiple acceptors around a central QD to increase the overall FRET efficiency.[1,3,5] Conversely, when brought in close proximity to dyes, gold nanoparticles (Au-NPs) allow effective fluorescence quenching over a broad range of wavelengths.[6−8] This suggests that QDs and Au-NPs could provide excellent donor−acceptor pairs. Interest in such pairs is further motivated by the potential of incorporating them into hybrid inorganic−biological nanostructures that can be optically interrogated.[1,9] To date, research has focused on developing methods to assemble and characterize structures that incorporate both QDs and Au-NPs and on their joint use to develop specific biosensors based on immunofluorescence or molecular beacons.[10−22] However, investigations aimed at probing the nature of the interactions between luminescent QDs and Au-NPs embedded in controlled assemblies, and how those interactions could affect the optical properties of these assemblies, remain rather limited. Furthermore, experimental studies probing the energy transfer from organic dye donors to Au−NP acceptors have provided somewhat inconsistent results.

There have been several analytical treatments describing the optical quenching of donor fluorophores by proximal Au-NPs, which can be loosely grouped into two sets based upon the postulated driving mechanism. One set applies the Förster dipole−dipole interaction model often referred to as FRET

* Corresponding author. E-mail: hedi.mattoussi@nrl.navy.mil.
† I.M. and T.P. contributed equally to this work.
‡ Present address: Ecole de Physique et Chimie Industrielle (ESPCI), Laboratoire Photons et Matière, CNRS UPRA0005, 10 Rue Vauquelin, 75005 Paris, France.
§ U.S. Naval Research Laboratory, Division of Optical Sciences.
|| U.S. Naval Research Laboratory, Center for Bio/Molecular Science and Engineering.
⊥ George Mason University.
University of Albany, State University of New York.
+ University of Maryland.

10.1021/nl071729+ CCC: $37.00 © 2007 American Chemical Society
Published on Web 09/11/2007

formalism.[14] The second set is based on approximating a dye−nanoparticle pair with a point dipole interacting with an infinite surface (nanosurface energy transfer, NSET).[23−27] Both descriptions treat energy transfer as an additional nonradiative pathway for the donor-excited-state decay and assume/predict no changes in the donor radiative rates.

To adapt the various concepts to the particular configuration where a single QD donor interacts with several acceptors (arrayed around its surface), we always consider multiple Au-NP quenchers interacting with a central point-dipole donor (e.g., an organic dye or a luminescent QD).[5] We also consider a fixed separation distance from the QD center to all NPs, but the treatment can be easily applied to a variable distance. We then express the donor quenching efficiency E as a function of the center-to-center separation distance R and the number N of gold nanoparticles interacting with a single donor using the general analytical expression[5,28]

$$E = \frac{Nk_{et}(R)}{k_r + k_{nr} + Nk_{et}(R)} = \frac{N}{\mathrm{N} + \left[\frac{k_r}{k_{et}(R)} \times \left(\frac{k_r + k_{nr}}{k_r}\right)\right]} \quad (1)$$

where k_r is the donor radiative rate, k_{et} is the energy transfer rate for a single (one-to-one) donor−acceptor pair, and k_{nr} is the rate accounting for all the other nonradiative pathways of the exciton decay. For QDs these pathways are often attributed to defects in the core crystalline structure and/or surface states. We will consider that these nonradiative pathways of the QD excitation are not affected by the interactions with proximal Au-NPs: $k_{nr} = k_{nr}{}^0$ in eq 1, as usually done when treating energy transfer configurations.

Within the Förster dipole−dipole description (FRET), the energy transfer rate exhibits a $1/R^6$ dependence[28]

$$E_{(\mathrm{FRET})} = \frac{N}{N + (R/R_{0(\mathrm{FRET})})^6}$$

$$R_{0(\mathrm{FRET})}{}^6 = \frac{9000\ln(10)}{N_A 128\pi^5}\frac{\kappa^2 \Phi_D{}^0 I}{n^4} \quad (2)$$

where $R_{0(\mathrm{FRET})}$ is the Förster separation distance, at which $E_{(\mathrm{FRET})}(N = 1) = 50\%$, n is the medium index of refraction, $\Phi^0{}_D$ is the quantum yield (QY) of the donor (for us, the QD) in the absence of acceptors (defined as $\Phi_D{}^0 = k_r{}^0/(k_r{}^0 + k_{nr}{}^0)$, and I is the spectral overlap integral between the normalized donor emission and the acceptor extinction coefficient. κ^2 is the dipole orientation factor, which becomes 2/3 for a random orientation of linear dipoles (e.g., dye−dye or QD−dye pairs).[28] In the case of Au-NP acceptors, assuming isotropic Au-NP polarizability and taking into account the conversion of the polarizability tensor into an extinction coefficient for computing the spectral overlap integral, a 2/3 value for the orientation factor results (see Supporting Information for further details). The Förster formalism has been widely used to describe nonradiative energy transfer for dye−dye donor−acceptor pairs[28] and has been applied to describe energy transfer between different size QDs embedded in close-packed films.[29] More recently there has been a flurry of bioinspired studies using QD donors coupled to dye acceptors via a protein/peptide or a membrane, where Förster dipole−dipole formalism was widely used to interpret the results.[1,5,30] Förster formalism has also been suggested as the dominant PL quenching mechanism for QDs conjugated to Au-NP-labeled oligonucleotides.[14]

An alternative model has recently been put forth by Govorov et al., who used a fluctuation−dissipation theorem to derive the nonradiative energy transfer rate between a semiconductor QD and a gold nanoparticle due to dipole−dipole coupling.[15,31] However, a close analysis of their energy transfer rate derived as a function of the QD radiative rate and the Au-NP extinction coefficient (e.g., eq 7 in ref 31) indicates that when the interparticle distance is larger than the particle sizes, $R > R_{\mathrm{Au-NP}}, R_{\mathrm{QD}}$ this treatment becomes equivalent to the Förster dipole−dipole model (eq 2 above). As this condition is usually satisfied in our self-assembled QD−peptide−Au-NP conjugates, we thus consider this treatment equivalent to the conventional Förster formalism.

Focusing on dye−Au-NP pairs and assuming a large difference in donor and acceptor dimensions, Strouse and co-workers proposed to abstract the system as a point dipole interacting with an infinite metal surface (nanosurface energy transfer, NSET).[25−27] Integrating the Förster expression over the two-dimensional surface leads to a $1/R^4$ dependence of the energy transfer rate

$$E_{(\mathrm{NSET})} = \frac{N}{N + (R/R_{0(\mathrm{NSET})})^4}$$

$$R_{0(\mathrm{NSET})}{}^4 = 0.225\frac{cn^2}{(2\pi)^2\omega_F k_F}\Phi_D{}^0\lambda_{QD}{}^2 \quad (3)$$

where $R_{0(\mathrm{NSET})}$ is now defined as the separation distance corresponding to 50% efficiency for $N = 1$, ω_F and k_F are the bulk gold angular frequency and Fermi vector, respectively, c is the velocity of light in vacuum, and λ_{QD} is the donor emission wavelength.

Finally, taking into account the finite size of the Au-NP and using Green formalism, Carminati et al. derived expressions for the distance dependence of the radiative and nonradiative rates from a point dipole interacting with proximal metallic nanoparticles (dipole-to-metal-particle energy transfer, DMPET).[32] Their treatment predicts no significant changes in the donor radiative rate, and an energy transfer efficiency $E_{(\mathrm{DMPET})}$ expressed as

$$E_{(\mathrm{DMPET})} = \frac{N}{N + (R/R_{0(\mathrm{FRET})})^6\left(1 + \frac{1}{6}(2\pi nR/\lambda_{QD})^2 + \frac{1}{6}(2\pi nR/\lambda_{QD})^4\right)^{-1}} \quad (4)$$

where $R_{0(\mathrm{FRET})}$ is the classical Förster radius as defined in eq 2. Equation 4 indicates that effects of the DMPET

treatment manifest as additional "correction terms" (to the quenching efficiency predicted by the Förster dipole−dipole model) that vary as $(R/\lambda_{QD})^2$ and (R/λ_{QD}).[4] However, since separation distances considered for energy transfer ($R \sim 1-30$ nm) are always smaller than λ_{QD} (400−800 nm), the additional contributions to Förster calculation become small (≤10%), with the highest correction expected at larger separation distance; at small distances the anticipated energy transfer efficiency is equivalent to the Förster model (eq 2).

In this report, we provide a detailed characterization of the fluorescence quenching of luminescent CdSe−ZnS core−shell QDs by proximal Au-NPs using QD−peptide−Au-NP conjugates. By combining metal-affinity-driven self-assembly with a series of rigid, Au-NP-labeled polypeptides, we achieve control over the center-to-center separation distance and number of Au-NPs arrayed around a single QD. We use steady-state and time-resolved PL measurements to determine the QD-to-Au-NP energy transfer efficiencies and compare the data to those derived for an identical sample configuration employing QD−peptide−organic dye conjugates. The data were used to test each of the formalisms described above and to compare and differentiate between mechanisms of QD fluorescence quenching induced by organic dye and metallic nanoparticle acceptors.

Results and Discussion. In order to evaluate QD PL quenching induced by proximal metallic nanoparticles and investigate the mechanism(s) involved, we exploit a relatively simple model system consisting of QD−peptide−Au-NP conjugates that allow placement of discrete numbers of Au-NPs around a single QD with control over the separation distances. To assemble such QD−Au-NP pairs, we utilize a series of engineered, variable-length de novo polypeptides which were shown to assume a rigid "rodlike" conformation.[33,34] Each peptide has a central block made up of several core β-strand repeat units, with tyrosine (Y), glutamic acid (E), histidine (H), and lysine (K) residues located at the turns of each unit. The peptides also express a C-terminal hexahistidine (His_6) tag and an N-terminal dicysteine group and are abbreviated by Cy_2-$YEHK_m$-His_6 (see materials section). The His_6 residues facilitate controlled polypeptide self-assembly onto the surface of CdSe−ZnS core−shell QDs, via metal-affinity interactions,[35] while the distal cysteine-thiols provide unique sites for modification with two monomaleimide-functionalized Au-NPs (as schematically represented in Figure 1).

We have previously utilized FRET measurements to characterize the conformation of dye-labeled-$YEHK_{1,3,5,7}$-His_6 (shorter sequences) polypeptides self-assembled onto DHLA-capped CdSe−ZnS core−shell QDs and found that in all cases studied the peptide rigid structure extending out from the surface was maintained after immobilization on the nanocrystal.[33] The peptide's rigid structure and spatial extension have also been confirmed by other structural and analytical measurements including Raman spectroscopy as well as atomic force and electron microscopy, see ref 34 and therein.

In the present study, we use the same family of rigid $YEHK_m$ polypeptides, albeit with longer core sequences (m = 5, 7, 14, 21) to evaluate QD PL quenching by proximal Au-NPs (Figure 1). The geometric QD-to-Au-NP center-to-center separation distance, R, for the different $YEHK_m$ were estimated using the QD and Au-NP radii, the sequence length of the beta-sheet, and assuming that the terminal histidine residues directly interact with the inorganic QD surface, as done in ref 33; R values are provided in Table 1 (additional details are provided in the Supporting Information). For each of the repeat sequences utilized, a mixture of Au-NP-labeled and unlabeled peptides were self-assembled onto QDs at a constant total ratio (12 per QD), while the fraction of Au-labeled peptides per QD conjugate was discretely varied. This configuration provides a measure of the quenching efficiency at several Au-NP-to-QD ratios for a given R while maintaining the average conjugate valence fixed, which improves the accuracy of our data.[5,36] Steady-state PL were measured for each set of QD−$YEHK_m$−Au-NP conjugate at various ratios and compared to those collected from control samples made of mixtures of Au-NPs and QD−$YEHK_m$ conjugates (unbound Au-NPs and QDs). These data were further complemented with time-resolved fluorescence measurements. Figure 2A shows a representative set of steady-state PL spectra collected from QDs conjugated to Au-NP-labeled

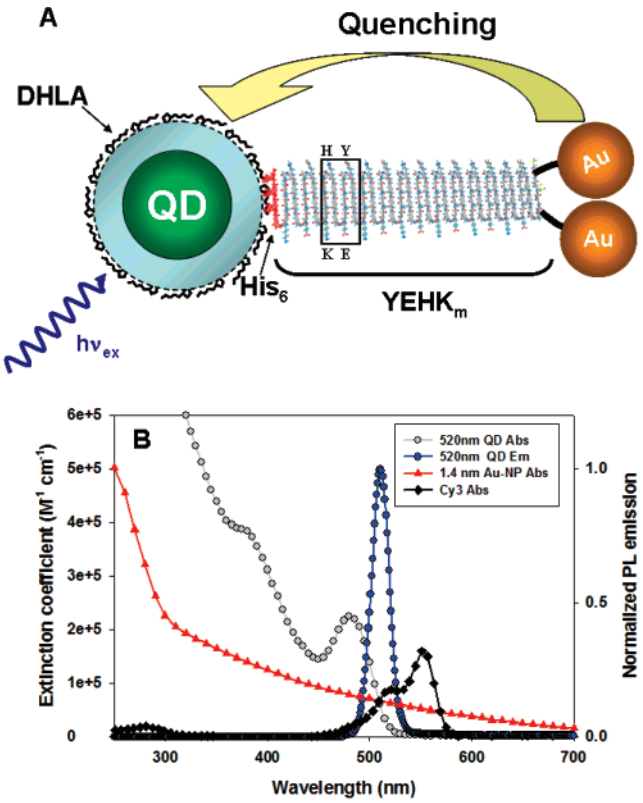

Figure 1. (A) Schematic representation of the QD−peptide−Au-NP bioconjugates. The C-terminal His_6 coordinates to the QD surface while the cysteines are used as attachment sites for 1.4 nm monomaleimide-functionalized Au-NPs. Repeat units of 5, 7, 14, or 21 were used; $YEHK_7$ as shown with a single core YEHK boxed. The Au-NPs are separated from the cysteine thiol by a maximum of ~8 Å and from each other by a maximum of 18 Å. (B) Extinction coefficient spectra of 520 nm emitting QDs, 1.4 nm Au-NPs and Cy3. Normalized emission of the QDs is also shown. The QY of the QD−$YEHK_m$ is ~20% and ϵ(420 nm) = 112000 M^{-1} cm^{-1} for the 1.4 nm Au-NPs.

Table 1. Measured PL Quenching Efficiencies for QD−YEHK$_m$−Au-NP Conjugates, Together with the Corresponding Radiative Rates k_r and Energy Transfer Rates k_{et} (Both Normalized by the Radiative Rate in the Absence of Au-NP, k_r^0)[a]

	YEHK$_5$	YEHK$_7$	YEHK$_{14}$	YEHK$_{21}$
QD to Au-NP distance R (Å)[b]	63 ± 1	93 ± 8	151 ± 10	212 ± 10
PL quenching	0.85 ± 0.06	0.50 ± 0.01	0.29 ± 0.01	0.11 ± 0.01
k_r/k_r^0		0.80 ± 0.17	1.12 ± 0.06	1.10 ± 0.05
k_{et}/k_r		4.6 ± 1.0	3.2 ± 0.3	1.2 ± 0.3

[a] Labeling ratios of three Au-NP on average per QD were used. Rates were derived as described in the text. [b] Center-to-center distance which includes the QD/Au-NP radii and Au-NP carbon linker.

YEHK$_7$ at increasing Au-NP-to-QD ratio. A pronounced and progressive quenching of QD PL is clearly measured as the ratio of Au-NP−YEHK$_7$-to-QD increased. The relative QD PL loss (i.e., quenching efficiency) vs ratio is fitted using eq 2 assuming a constant R for a given set of QD−YEHK$_m$−Au-NP conjugates (Figure 2B). This suggests absence of collective quenching due to inter-Au-NP interactions and implies that within a conjugate the QD interacts individually with each proximal Au-NP and independent of the presence of other nanoparticles. In comparison control samples showed little to no PL quenching, indicating that contributions from solution-phase (dynamic quenching) or nonspecific interactions are essentially negligible (Supporting Information, Figure S1). Time-resolved data shown in Figure 2C indicate that there is a significant decrease in QD excited-state lifetime upon conjugation to Au-NP-labeled-YEHK$_7$. Similar and specific quenching was also measured for other color/size QDs upon conjugation with YEHK$_m$−Au-NPs (data not shown).

To account for the effects of Au-NPs on the decay rates, we introduce an additional decay channel due to ET (with a rate k_{et}) and assume that the QD PL nonradiative pathways (other than ET) are not affected by the Au-NP presence, $k_{nr} = k_{nr}^0$. Using the expression of the QY as a function of the decay rates (ref 25 and Supporting Information), we derive relations that account for the changes in the radiative and nonradiative rates of the QD excitation (after assembly with Au-NPs) as a function of k^0 and k

$$\frac{k_r}{k_r^0} = \frac{\Phi}{\Phi^0}\frac{k_r + k_{nr} + k_{et}}{k_r^0 + k_{nr}^0} = \frac{\Phi}{\Phi^0}\frac{k}{k^0} \tag{5}$$

$$\frac{k_{et}}{k_r} = \left(\frac{1-\Phi}{\Phi}\right) - \left(\frac{1-\Phi^0}{\Phi^0}\right)\frac{k_r^0}{k_r} \tag{6a}$$

or

$$\frac{k_{et}}{k_r} = \left(\frac{1-\Phi}{\Phi}\right) - \left(\frac{1-\Phi^0}{\Phi}\right)\frac{k^0}{k} \tag{6b}$$

using eq 5. Combining steady-state data (Φ values) and time-resolved QD PL measurements (decay rates), we extracted estimates for the normalized radiative and energy transfer decay rates (using eqs 5 and 6) for the QD−YEHK$_m$−Au-NP conjugates and probed their dependence on the separation distance R. Values for those normalized rates are summarized in Table 1. Data indicate that the radiative decay rates derived for the QD−YEHK$_m$ conjugates are essentially unchanged in the presence or absence of Au-NPs ($k_r/k_r^0 \sim 1$), even when the QD PL quenching is very efficient. Small deviations from $k_r/k_r^0 \sim 1$ may be attributed to the difficulty in deriving a QD decay rate due to the complex nonexponential PL decay kinetics.[37] Conversely, the derived ET rate is significantly higher than the radiative rate ($k_{et}/k_r > 1$) and progressively decreases with increasing separation distance. These observations confirm that while the QD donor radiative rate is relatively unchanged, as expected for these distances from the three models considered here, the presence of Au-NPs introduces an additional nonradiative pathway for the QD exciton recombination.[32] This is similar to the results reported for a fluorescein dye−Au-NP system.[27] However, it contrasts with other previous studies of dye−Au-NP interactions, where a decrease in the dye radiative rates was suggested to be the major cause of dye PL quenching.[38,39] Such disagreement may arise (partially) from differences in the sample configuration used. Those two studies used larger Au-NPs (which have marked plasmon resonance absorbance) and high dye-to-Au-NP ratios, compared to the NPs and sample configuration used in the current work and in ref 27.

We have previously shown that "inhomogeneous" wavelength-dependent PL quenching of a QD dispersion can be characteristic of resonant energy transfer processes between QDs and proximal dyes.[40] We attributed this process to an inhomogeneous donor−acceptor spectral overlap, $J(\lambda)$, across the PL spectrum of a macroscopic QD sample: $J(\lambda) \sim \epsilon(\lambda)\lambda^4$; $\epsilon(\lambda)$ being the wavelength-dependent extinction coefficient. The PL spectrum of a colloidal QD population (in a homogeneous sample) is composed of a continuum of very narrow single QD spectra (10−15 nm at room temperature), due to inhomogeneities in nanocrystal size within the population and the color-size dependency imposed by carrier quantum confinement effects.[41,42] We have demonstrated that this allows investigation of the wavelength-dependent interactions between QDs and FRET acceptors. In particular, we showed that the "bluer" fraction of QDs within a population may be quenched with a different efficiency than their "redder" counterparts, with exact levels of quenching depending on the relative positions of the QD ensemble PL and acceptor absorption spectra. In some cases, this has produced a deformation of the QD ensemble PL spectrum, which we used to deduce information on the wavelength dependence of the QD quenching mechanism (see ref 40 and Supporting Information for additional details). Applying

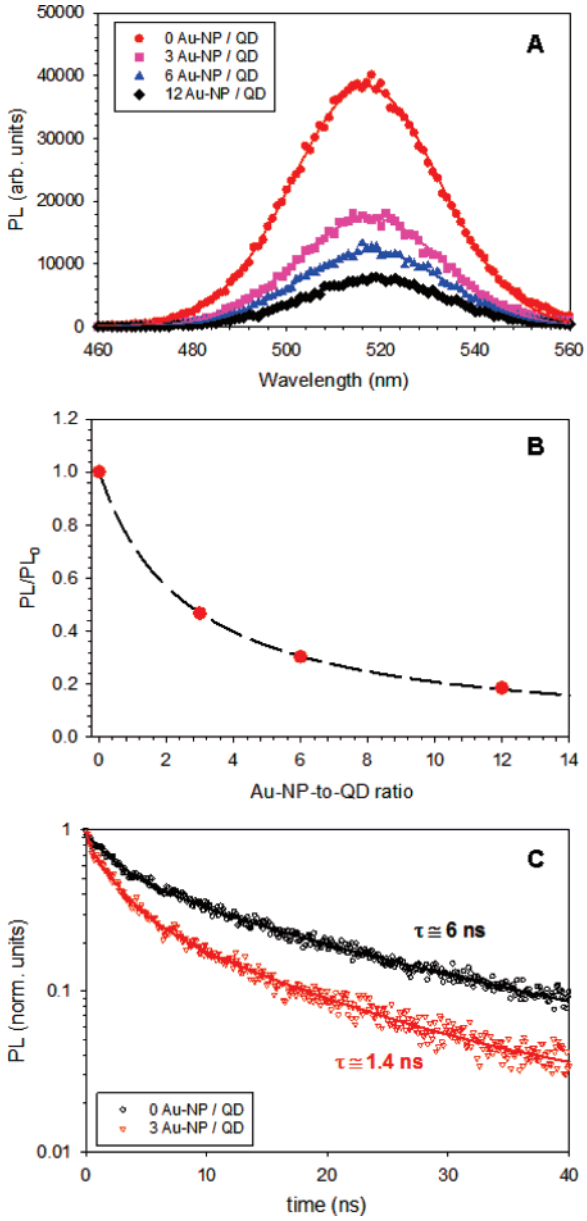

Figure 2. (A) PL spectra collected from QD−YEHK$_7$−Au-NP conjugates using 300 nm excitation. (B) Plot of normalized PL loss (PL/PL$_0$) as a function of the number of YEHK$_7$−Au-NP per QD from data in (A). (C) Plot of time-resolved fluorescence for 520 nm QDs vs elapsed time in the absence and in the presence of 3-YEHK$_7$−Au-NP per QD conjugate. The solid lines are fits to the data using a three-exponential-decay function, as described in the text.

those concepts to the present sample configuration, we anticipate that within the QD emission spectrum a PL quenching rate proportional to $\epsilon_{Au-NP}(\lambda)\lambda^4$ will be measured for FRET (eq 2), whereas a rate proportional to λ^2 (eq 3) should be measured for NSET. Figure 3 shows the measured wavelength-dependent QD PL quenching rate for the QD−Au-NP conjugates used together with the quenching rates anticipated from the different models; PL spectra of the QDs alone and QD−peptide−Au-NP conjugates are also shown for comparison. Data indicate that the wavelength dependence of the measured quenching rate across the QD PL spectrum is in better agreement with NSET predictions.

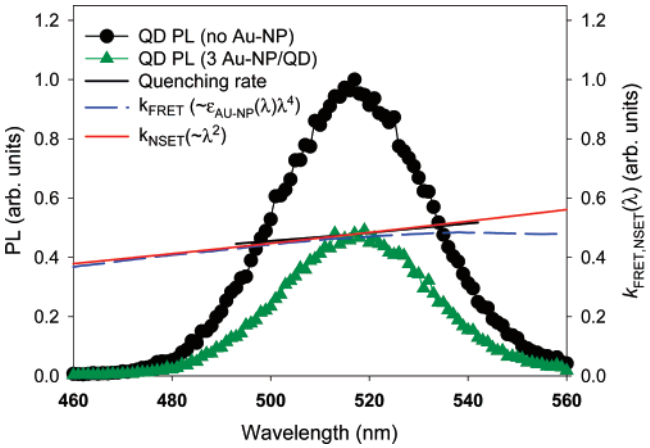

Figure 3. PL spectra corresponding to QDs alone (black dots) and QDs conjugated with three YEHK$_7$−Au-NPs (green triangles). Also shown are the experimental wavelength-dependent quenching rate (black line), along with the predictions for the transfer rate from NSET with a rate proportional to λ^2 (red line) and FRET with a rate proportional to $\epsilon_{Au-NP}(\lambda)\lambda^4$ (blue line).

Figure 4A shows a plot of the QD quenching efficiency for each of the Au-NP−YEHK$_m$ tested, as a function of the nominal QD−YEHK$_m$−Au-NP separation distance together with data collected for QD−YEHK$_{1,3,5,7,14,21}$−Cy3 (including the current peptide series and the previously mentioned shorter ones reproduced from ref 33). Additionally, quenching efficiencies measured for QD−ds-DNA−Au-NP conjugates from ref 14 are reproduced for comparison. This allowed a comprehensive analysis of the results by comparing effects of separation distances and whether metallic particles or organic dyes were used; all data are normalized for quenching efficiencies at $N = 1$. We also fit the experimental data to the FRET, NSET, and DMPET analytical treatments introduced above (eqs 2−4), using two forms of comparison. In Figure 4A, the comparison between fits and data was carried using R_0 as a fitting parameter, whereas in Figure 4B comparison to the fits was carried out using R_0 values extracted from the experimental parameters, namely, ϕ_D^0 and overlap integral (eqs 2 and 3). Table 2 shows R_0 values extracted from the fits (in Figure 4A) together with those derived experimentally. Use of R_0 as a fitting parameter (in Figure 4A) is essentially an indirect approach of accounting for errors associated with estimates of this parameter using experimental data such as quantum yield and overlap integral. In close examination of these plots and the corresponding fits, three conclusions can be drawn:

(1) The PL quenching efficiency decreases steadily as the QD-to-Au-NP separation distance increases. Our experimental observations are consistent with the results reported for QD−ds-DNA−Au-NP conjugates in ref 14. Moreover, our data significantly extend the range of accessible separation distances to investigate the PL quenching induced by metallic Au-NPs.

(2) The QD PL quenching induced by proximal Au-NPs persists over long separation distances, with significant PL loss measured at separation distances extending beyond 200 Å.[27] It is also much more pronounced than what was measured for energy transfer to Cy3 dye acceptors (for which

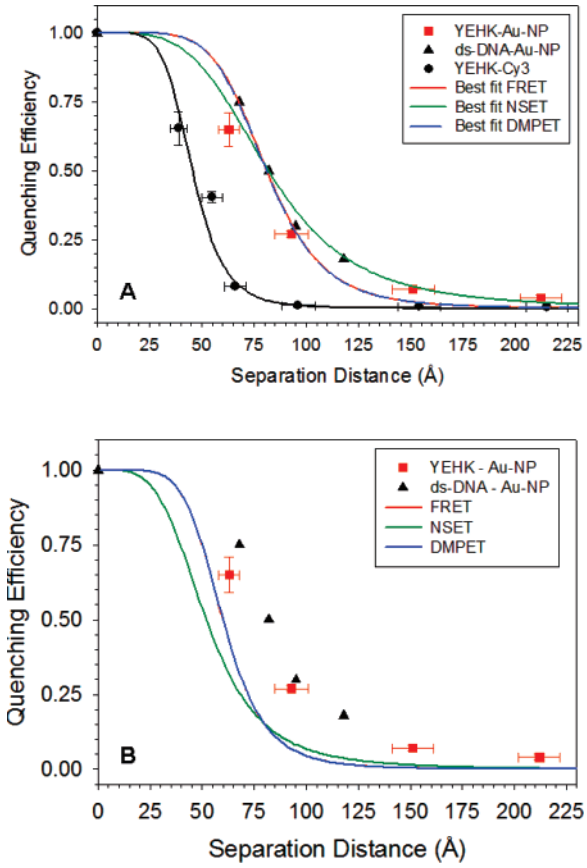

Figure 4. PL quenching efficiency vs R for QD−YEHK$_{5,7,14,21}$−Au-NP conjugates (red squares) and QD−dsDNA−Au-NP from ref 14 (black triangles) together with best fits using FRET (red line), DMPET (blue line), and NSET (green line). The quenching efficiencies for QD−YEHK$_{1,3,5,7,14,21}$−Cy3 conjugates from ref 33 along with a fit using Förster FRET formalism are also shown (black dots and back line). Comparison between fits and data using R_0 either as a fitting parameter (A), or the experimental values deduced form the spectral overlap and QY (B). Center-to-center distances are slightly larger for the QD−peptide−Cy3 conjugates due to the presence of a larger dye linker. Horizontal error bars are the standard deviation of the distance and vertical error bars are the standard deviation of the measurement. Note that in the two panels FRET and DMPET fits overlap over the full range of distances explored.

Table 2. Best Fit and Predicted R_0 Parameters (Å) Corresponding to the Three Energy Transfer Models[a]

energy transfer model	quenching rate distance dependence	best fit R_0 (Å)	$R_{0\|exp}$ (Å)
FRET (eq 2)	$1/R^6$	80	60 (eq 2)
NSET (eq 3)	$1/R^4$	80	52 (eq 3)
DMPET (eq 4)	$\sim 1/R^6$	80	60 (eq 2)

[a] The experimental values for R_0 were derived using $\phi_D = 0.2$ for the QD−YEHK$_m$ conjugates.

$R_0 \cong 51$ Å). For example, the quenching efficiency for QD−YEHK$_5$−Au-NP bioconjugates is 65% compared to 8% measured for solutions of QD−YEHK$_5$−Cy3 conjugates, about an order of magnitude difference. Similarly, at a separation distance of ~80 Å where the PL quenching due to Förster dipole−dipole (FRET) interactions becomes negligible for most conventional dye−dye pairs,[28] the quenching efficiency for the QD−Au-NP pair is ~50%. The difference cannot be attributed to a disparity in the extinction coefficients, since 1.4 nm Au-NPs and Cy3 have similar extinction coefficients at 520 nm (PL peak of the QDs used, see Figure 1).

(3) In comparison, the Förster dipole−dipole formalism (which assumes a random dipole orientation factor, $\kappa^2 = 2/3$) provides an excellent fit to the experimental quenching efficiencies measured for QD−YEHK$_{1,3,5,7,14,21}$−Cy3 conjugates. This data set confirms that Förster (dipole−dipole) energy transfer dominates interactions between luminescent QDs and proximal dyes, with a resulting $1/R^6$ dependence of the FRET rate.

We now discuss the above set of data within the framework of the theoretical treatments introduced above, namely, FRET, DMPET, and NSET. In particular, we evaluate both the ability of the treatments to correctly predict the shape of the PL quenching versus distance curve and the validity of the parameters extracted from the various fits (using eqs 2−4). Figure 4A shows that when R_0 is used as a fitting parameter (i.e., allowed to vary), the NSET model (with its weaker dependence on R) provides a better fit to the data at longer separation distances (beyond 100 Å) than FRET and DMPET. The values for R_0 extracted from fits to all three treatments (Figure 4A) are larger than those derived using the experimental conditions, or equivalently, the quenching efficiencies predicted are smaller than those measured. In comparison, the predictions of the Förster mechanism underestimated values at larger distances. This is consistent with what has been demonstrated previously for dye−Au-NP systems.[25−27] Interestingly, we find that the quenching data derived by Gueroui et al.[14] (where a more narrow range of separation distances was explored) can be fitted using all three models with reasonable agreement (Figure 4A). However, when the experimental R_0 values are used to fit the quenching data (Figure 4B), the three models predict smaller quenching efficiencies than what was measured. The difference between experimental and predicted quenching efficiency may be attributed (only partially) to uncertainties in the QD concentration and/or errors in the measured QY for the QD conjugates. Finally, we cannot rule out the possibility that quenching mechanisms other than dipole−dipole coupling (including charge transfer-induced processes) exist and may also contribute to the measured PL quenching of the nanocrystals. Overall, QDs are larger size fluorophores than conventional dyes, with PL that tends to be influenced by surface properties and large surface-to-volume ratios, and their interactions with metallic NPs may be more complicated than those of small size dyes.

Overall, the NSET treatment appears to provide a better description (though not very quantitative) of the experimental quenching of QDs by proximal Au nanoparticles. As a matter of fact rather good agreements between predictions of NSET and experiments were reported for dye−Au-NP pairs (see refs 25-27). In comparison, FRET (and DMPET) underestimates the rate of quenching and is also unable to describe the trend observed at longer separation distances, while NSET can describe the trend of the quenching data at larger R, while concurrently underestimating the efficiency values.

With reference to the physical origin of the models, we note that the NSET treatment essentially relies on approximating the Au-NPs as infinite surfaces with respect to a smaller dye donor. While this might be reasonable for small separation distances and large Au-NPs, the experimental QD PL quenching we measured extends over distances that are much larger than the nanoparticle size (~150 times the Au-NP size). Additionally, NSET anticipates a quenching rate that is independent of the Au-NP size, although more efficient quenching is expected with larger gold particles (for example compare results reported in refs 25 and 43).

Conclusion. In this report we have examined the quenching of luminescent CdSe−ZnS quantum dots due to interactions with proximal Au nanoparticles conjugated to the nanocrystal surface by rigid, variable-length peptides. By using a combination of easy to implement self-assembly and rigid beta-sheet peptides, we were able to achieve two unique features: (1) varying the ratio of Au-NP-to-QD in a given QD−YEHK$_m$−Au-NP conjugate sample, and (2) discretely spanning a broad range of separation distances by varying the number of repeat units *m* from one conjugate series to another. We found that Au-NP driven QD PL quenching extends over a large distance range, much larger than what was predicted and measured for dye−dye and QD-dye pairs.[1,25] Combining this with the ability to array multiple Au-NPs around a central QD, it may be possible to extend the energy transfer rate and the utility of sensors based on this pair to separation distances of ~200 Å, far beyond the range allowed by "classic" dye-to-dye FRET pairs.[1,3,9,28] Indeed it is well worth noting that many of the QD−Au-NP sensing assemblies referenced here would most likely not function using organic dye acceptors, due to the size constraints imposed by rather large encapsulated QD donors.[10,12,14,18,22]

Using a close comparison of the predominant descriptive theories, we found that cumulatively the QD PL quenching is mainly due to nonradiative energy dissipation by the Au-NP without any significant modifications of the QD radiative rate. The long distance quenching rate is better described with a slower distance-dependence quenching rate than the classical $1/R^6$ characteristic of Förster energy transfer. We also found that the dipole to metal nanoparticle energy transfer (NSET) model[32] provides a better description of the distance dependence of the quenching efficiencies, even though agreement is only qualitative since the measured values were always larger than the predicted ones. Further studies are still needed to provide a better understanding of the mechanisms driving the pronounced PL quenching of dyes and QDs alike by proximal metallic nanoparticles. Our findings also indicate that these systems, with their ability to allow long-range quenching of QD photoemission, could provide effective platforms for designing sensors with applicability in both *in vitro* and *in vivo* studies.

Experimental Section. Polypeptide Labeling with Au-NPs and QD-Conjugate Self-Assembly. The design and recombinant construction of the polypeptides is detailed extensively in ref 44. The polypeptides used here consist of an N-terminal dicysteine and C-terminal hexahistidine (His$_6$) sequence attached at the ends of a central block made up of a variable number of core β-strand repeat units, with tyrosine (Y), glutamic acid (E), histidine (H), and lysine (K) residues located at the turns of each unit; polypeptides are designated by YEHK$_m$ where *m* is the number of core repeat units.[33] The YEHK$_m$ polypeptides were expressed in bacterial host strains and purified as previously described.[33] Following purification, the peptides were reduced with dithiothreitol and labeled with monomaleimide-functionalized 1.4 nm size gold nanoparticles (Nanoprobes, Yaphank, NY) according to the manufacturer's protocol. Au-NP labeled YEHK$_m$ polypeptides were purified over Sephadex 200 media (GE Healthcare, Piscataway NJ) and quantitated using UV−vis spectroscopy. Absorption spectra of Au-NP labeled YEHK$_m$ were consistent with the spectra for isolated YEHK$_m$ and free Au-NPs, indicating absence of aggregate formation in solution. Average labeling ratios of 1.5 Au-NP per polypeptide sequence were deduced from the absorption data and the plasmonic extinction coefficient of Au-NPs at 420 nm (112000 M^{-1} cm^{-1}).

For conjugate assembly, QDs were added to a mixture of labeled and unlabeled peptides (at the appropriate molar ratios) in 10 mM NaTetraborate buffer, pH 9.5, and allowed to react for at least 1 h prior to assaying; final QD concentration in the assays was 0.2 μM. This permitted self-assembly of both Au-NP labeled and unlabeled polypeptides on the QD surface.[45] For both quenching and lifetime experiments the total number of YEHK$_m$ polypeptides self-assembled per QD was maintained at 12 while the ratio of Au-NP labeled to unlabeled polypeptide was varied. PL spectra were collected on a Tecan Safire Dual Monochromator Multifunction Microtiter Plate Reader (Tecan, Research Triangle Park, NC). Samples were measured in triplicate, and error bars are shown where appropriate. The CdSe−ZnS core−shell QDs with an emission maxima centered around 520 nm were synthesized in our laboratory using high-temperature reaction of organometallic precursors followed by cap exchange with dihydrolipoic acid (DHLA) as described in ref 46.

Time-Resolved Measurements. Time-resolved QD PL decays were acquired using a home-built time-correlated single photon counting (TCSPC) setup equipped with a modelocked tunable (from 920 to 710 nm) titanium sapphire laser source with a repetition rate of 80 MHz (Wideband Mai Tai, Newport Corp.), as described in ref 47. The 800 nm line was frequency-doubled (using a barium borate crystal, Photop Technologies) to provide a pulsed excitation line at 400 nm used in all our experiments. Typical instrument response functions had a full width at half-maximum of 45 ps. PL decay curves could not be modeled by single exponential decays due to the complexity of the QD photophysics[37] but could be fitted using three monoexponential decays. No improvement in the fitting accuracy was obtained when using a higher number of monoexponential decays. The decay rate *k* is derived as the average of the individual component rates, weighted by their respective amplitude.

Acknowledgment. I.L.M., T.P., K.E.S. and H.M. acknowledge NRL and L. Chrisey at the Office of Naval Research (Grant No. N001404WX 20270) and Stephen Lee and Ilya Elashvilli of the CB Directorate/Physical S&T Division, DTRA for support. T.P. acknowledges a postdoctoral fellowship from the Fondation pour la Recherche Médicale (France). S.H. is pleased to acknowledge the generous support of the Office for Research of the University at Albany. Instrumentation for this work was provided by an NSF-CRIF award (CHE-0342973) to D.S.E.

Supporting Information Available: Derivation of the orientation factor κ^2 for QD−Au-NP assemblies, estimation of center-to-center separation distances, definition of decay rates, control experiments accounting for QD quenching by free Au-NPs, and spectrally resolved QD PL quenching by Au-NPs. This material is available free of charge via the Internet at http://pubs.acs.org.

References

(1) Clapp, A. R.; Medintz, I. L.; Mattoussi, H. *ChemPhysChem.* **2005**, *7*, 47.
(2) Michalet, X.; Pinaud, F. F.; Bentolila, L. A.; Tsay, J. M.; Doose, S.; Li, J. J.; Sundaresan, G.; Wu, A. M.; Gambhir, S. S.; Weiss, S. *Science* **2005**, *307*, 538.
(3) Medintz, I. L.; Uyeda, H. T.; Goldman, E. R.; Mattoussi, H. *Nat. Mater.* **2005**, *4*, 435.
(4) Zhang, C. Y.; Yeh, H. C.; Kuroki, M. T.; Wang, T. H. *Nat. Mater.* **2005**, *4*, 826.
(5) Clapp, A. R.; Medintz, I. L.; Mauro, J. M.; Fisher, B. R.; Bawendi, M. G.; Mattoussi, H. *J. Am. Chem. Soc.* **2004**, *126*, 301.
(6) Burda, C.; Chen, X. B.; Narayanan, R.; El-Sayed, M. A. *Chem. Rev.* **2005**, *105*, 1025.
(7) Daniel, M. C.; Astruc, D. *Chem. Rev.* **2004**, *104*, 293.
(8) Dubertret, B.; Calame, M.; Libchaber, A. J. *Nat. Biotechnol.* **2001**, *19*, 365.
(9) Sapsford, K. E.; Berti, L.; Medintz, I. L. *Angew. Chem., Int. Ed.* **2006**, *45*, 4562.
(10) Oh, E.; Hong, M. Y.; Lee, D.; Nam, S. H.; Yoon, H. C.; Kim, H. S. *J. Am. Chem. Soc.* **2005**, *127*, 3270.
(11) Dyadyusha, L.; Yin, H.; Jaiswal, S.; Brown, T.; Baumberg, J. J.; Booy, F. P.; Melvin, T. *Chem. Commun.* **2005**, 3201.
(12) Chang, E.; Miller, J.; Sun, J.; Yu, W.; Colvin, V.; Drezek, R.; West, J. *Biochem. Biophys. Res. Commun.* **2005**, *334*, 1317.
(13) Fu, A. H.; Micheel, C. M.; Cha, J.; Chang, H.; Yang, H.; Alivisatos, A. P. *J. Am. Chem. Soc.* **2004**, *126*, 10832.
(14) Gueroui, Z.; Libchaber, A. *Phys. Rev. Lett.* **2004**, *93*.
(15) Slocik, J. M.; Govorov, A. O.; Naik, R. R. *Supramol. Chem.* **2006**, *18*, 415.
(16) Biju, V.; Itoh, T.; Makita, Y.; Ishikawa, M. *J. Photochem. Photobiol., A* **2006**, *183*, 315.
(17) Wargnier, R.; Baranov, A. V.; Maslov, V. G.; Stsiapura, V.; Artemyev, M.; Pluot, M.; Sukhanova, A.; Nabiev, I. *Nano Lett.* **2004**, *4*, 451.
(18) Cady, C. N.; Strickland, A. D.; Batt, C. A. *Mol. Cell. Probes* **2007**, *21*, 116.
(19) Liu, N. G.; Prall, B. S.; Klimov, V. I. *J. Am. Chem. Soc.* **2006**, *128*, 15362.
(20) Eckel, R.; Walhorn, V.; Pelargus, C.; Martini, J.; Enderlein, J.; Nann, T.; Anselmetti, D.; Ros, R. *Small* **2007**, *3*, 44.
(21) Slocik, J. M.; Tam, F.; Halas, N. J.; Naik, R. R. *Nano Lett.* **2007**, *7*, 1054.
(22) Liu, J.; Lee, J. H.; Lu, Y. *Anal. Chem.* **2007**, *79*, 4120.
(23) Chance, R. R.; Prock, A.; Silbey, R. Molecular fluorescence and energy transfer near interfaces. In *Advances in Chemical Physics*; J. Wiley & Sons: New York, 1978; Vol. 37; p 1.
(24) Persson, B. N. J.; Lang, N. D. *Phys. Rev. B* **1982**, *26*, 5409.
(25) Yun, C. S.; Javier, A.; Jennings, T.; Fisher, M.; Hira, S.; Peterson, S.; Hopkins, B.; Reich, N. O.; Strouse, G. F. *J. Am. Chem. Soc.* **2005**, *127*, 3115.
(26) Jennings, T. L.; Schlatterer, J. C.; Singh, M. P.; Greenbaum, N. L.; Strouse, G. F. *Nano Lett.* **2006**, *6*, 1318.
(27) Jennings, T. L.; Singh, M. P.; Strouse, G. F. *J. Am. Chem. Soc.* **2006**, *128*, 5462.
(28) Lakowicz, J. R. *Principles of Fluorescence Spectroscopy*, 3rd ed.; Springer: New York, 2006.
(29) Kagan, C. R.; Murray, C. B.; Nirmal, M.; Bawendi, M. G. *Phys. Rev. Lett.* **1996**, *76*, 1517.
(30) Patolsky, F.; Gill, R.; Weizmann, Y.; Mokari, T.; Banin, U.; Willner, I. *J. Am. Chem. Soc.* **2003**, *125*, 13918.
(31) Govorov, A. O.; Bryant, G. W.; Zhang, W.; Skeini, T.; Lee, J.; Kotov, N. A.; Slocik, J. M.; Naik, R. R. *Nano Lett.* **2006**, *6*, 984.
(32) Carminati, R.; Greffet, J.-J.; Henkel, C.; Vigoureux, J. M. *Opt. Commun.* **2006**, *261*, 368.
(33) Medintz, I. L.; Sapsford, K. E.; R., C. A.; Pons, T.; Higashiya, S.; Welch, J. T.; M., M. H. *J. Phys. Chem. B* **2006**, *110*, 10683.
(34) Topilina, N. I.; Higashiya, S.; Rana, N.; Ermolenkov, V. V.; Kossow, C.; Carlsen, A.; Ngo, S. C.; Wells, C. C.; Eisenbraun, E. T.; Dunn, K. A.; Lednev, I. K.; Geer, R. E.; Kaloyeros, A. E.; Welch, J. T. *Biomacromolecules* **2006**, *7*, 1104.
(35) Sapsford, K. E.; Pons, T.; Medintz, I. L.; Higashiya, S.; Brunel, F. M.; Dawson, P. E.; Mattoussi, H. *J. Phys. Chem. C* **2007**, *111*, 11528.
(36) Pons, T.; Medintz, I. L.; Wang, X.; English, D. S.; Mattoussi, H. *J. Am. Chem. Soc.* **2006**, *128*, 15324.
(37) Schlegel, G.; Bohnenberger, J.; Potapova, I.; Mews, A. *Phys. Rev. Lett.* **2002**, *88*.
(38) Dulkeith, E.; Morteani, A. C.; Niedereichholz, T.; Klar, T. A.; Feldmann, J.; Levi, S. A.; van Veggel, F.; Reinhoudt, D. N.; Moller, M.; Gittins, D. I. *Phys. Rev. Lett.* **2002**, *89*.
(39) Schneider, G.; Decher, G.; Nerambourg, N.; Praho, R.; Werts, M. H. V.; Blanchard-Desce, M. *Nano Lett.* **2006**, *6*, 530.
(40) Pons, T.; Medintz, I. L.; Sykora, M.; Mattoussi, H. *Phys. Rev. B* **2006**, *73*, 245302.
(41) Empedocles, S. A.; Norris, D. J.; Bawendi, M. G. *Phys. Rev. Lett.* **1996**, *77*, 3873.
(42) Artemyev, M. V.; Woggon, U.; Wannemacher, R.; Jaschinski, H.; Langbein, W. *Nano Lett.* **2001**, *1*, 309.
(43) Ray, P. C.; Fortner, A.; Darbha, G. K. *J. Phys. Chem. B* **2006**, *110*, 20745.
(44) Higashiya, S.; Topilina, N. I.; Ngo, S. C.; Zagorevskii, D.; Welch, J. T. *Biomacromolecules* **2007**, *8*, 1487.
(45) Medintz, I. L.; Clapp, A. R.; Mattoussi, H.; Goldman, E. R.; Fisher, B.; Mauro, J. M. *Nat. Mater.* **2003**, *2*, 630.
(46) Mattoussi, H.; Mauro, J. M.; Goldman, E. R.; Anderson, G. P.; Sundar, V. C.; Mikulec, F. V.; Bawendi, M. G. *J. Am. Chem. Soc.* **2000**, *122*, 12142.
(47) Grimes, A. F.; Call, S. E.; Vicente, D. A.; English, D. S.; Harbron, E. J. *J. Phys. Chem. B* **2006**, *110*, 19183.

NL071729+